Theoretical Studies on Structures and Spectroscopic Properties of Cyclometalated Gold(III) Complexes

Bao-Zhu Yang, Xin Zhou, Tao Liu, Fu-Quan Bai, and Hong-Xing Zhang*

State Key Laboratory of Theoretical and Computational Chemistry, Institute of Theoretical Chemistry, Jilin University, Changchun 130023, People's Republic of China

Received: December 12, 2008; Revised Manuscript Received: June 1, 2009

The electronic structures and spectroscopic properties of the four tridentate cyclometalated Au(III) complexes [Au(ĈN̂C)C≡CPh] (**1**), [Au(N̂ĈC)C≡CPh] (**2**), [Au(N̂N̂C)C≡CPh]$^+$ (**3**), and [Au(N̂ĈN)C≡CPh]$^+$ (**4**) [HĈN̂CH = 2,6 -diphenylpyridine, N̂CĤCH = 3-(2-pyridyl)biphenyl, N̂N̂CH = 6-phenyl-2,2′- bipyridine, N̂CHN̂ = 1,3-di(2-pyridyl)benzene] were calculated to explore their spectroscopic nature. The geometry structures of **1**−**4** in the ground and excited states were optimized under the density functional theory (DFT) and the single-excitation configuration interaction (CIS) level, respectively. The absorption and emission spectra in CH_2Cl_2 solution were calculated by the time-dependent density functional theory (TD-DFT) with the PCM solvent model. As revealed from the calculations, with the variation of pyridyl in position and the number, the electron-accepting ability of pyridyl in **1**−**4** are different. With increasing the electron-accepting ability of pyridyl, the HOMO−LUMO energy gaps of **1**−**4** decrease, and the lowest-energy absorption bands and emission bands are red-shifted in the order **1** < **2** < **4** < **3**. All of the lowest-energy absorptions are assigned as the LLCT character, and the solvent polarity has little impact on the absorption spectra. The 477 nm emission of **1** arises from the ^{3}ILCT transition, whereas the 517 and 634 nm emission of **2** and **3**, respectively, come from the ^{3}LLCT and ^{3}ILCT. In addition, the 577 nm emission of **4** is assigned as ^{3}LLCT/^{3}LMCT character.

1. Introduction

During the past few decades, great attention has been paid to the development of phosphorescent materials, because of their potential application as highly efficient electroluminescent (EL) emitters in organic light emitting devices (OLEDs).[1] In particular, late transition metal with the d^6 and d^8 electronic configuration (such as platinum(II),[2] iridium(III),[3] osmium(II),[4] ruthenium(II),[5] and aurum(I)[6]) have been widely applied in the exploration of OLEDs. These complexes usually display long-lived emission and high luminescent efficiency. According to the transition principle, only the transitions arising from spin-allowed $S_0 \rightarrow S_n$ can result in luminescence, and spin-forbidden $S_0 \rightarrow T_n$ transitions are inhibited in nature and consequently nonluminescent. However, because of the strong spin−orbit coupling effect of the heavy metal, which increases the rate of $S_1 \rightarrow T_1$ intersystem crossing, the phosphorescence originating from the triplet excited states can be achieved.

In recent years, gold(I) complexes have been the subject of some intense researches, such as in the weak metal−metal interactions and the interesting photophysical and photochemical properties;[6,7] a lot of in-depth studies in experiments and theoretical calculations have been done. In contrast to the gold(I) system, most of the gold(III) complexes usually emit at low temperature in the solid state or glasses, with very few examples emitting at room temperature in solution. One probable reason for the behavior in gold(III) complexes is the presence of low-energy radiationless d-d states, which compete with the charge transfer transition and result in weak luminescence or nonluminescence at room temperature. As a consequence, very few cases of luminescent gold(III) complexes were reported.[8]

Recently, a series of luminescent alkynylgold(III) complexes, [Au(ĈN̂C)(C≡CR)] (HĈN̂CH=2,6-diphenylpyridine), were synthesized and structurally characterized by Yam and co-workers.[9] The complexes represent isoelectronic and structural analogues of alkynylplatinum(II) terpyridyl, [Pt(N̂N̂N)(C′CR)]$^+$ (N̂N̂N = 2,2′,6′,2″-terpyridine),[1d,10] and cyclometalated complexes, [Pt(N̂N̂C)(C≡CR)] (N̂N̂CH=6-phenyl-2,2′-bipyridine).[11] Unlike most other gold(III) complexes, which are nonemissive at room temperature or only show luminescence at low temperature, the complexes display intense phosphorescence at 470−611 nm on excitation at $\lambda \geq 360$ nm at both room temperature and 77 k. Furthermore, the novel class of luminescent alkynylgold(III) complexes has been demonstrated possessing EL properties and has been employed as electrophosphorescent emitters or dopants of OLEDs with high brightness and efficiency.[9b] The similar study of Ir complexes has been carried out by Scandola et al.[3c] and Williams et al.,[3d] and the corresponding photophysical and photochemical properties have been explored in details.

Although there have been some reports about the photophysical and photochemical properties of alkynylgold(III) complexes,[8,9] corresponding theoretical researches are sparse. Herein, a detailed theoretical investigation on the electronic structures and spectra of the complexes [Au(ĈN̂C)C≡CPh] (**1**), [Au(N̂ĈC)-C≡CPh] (**2**), [Au(N̂N̂C)C≡CPh]$^+$ (**3**), and [Au(N̂ĈN)C≡CPh]$^+$ (**4**) (HĈN̂CH=2,6-diphenylpyridine, N̂CĤCH=3-(2-pyridyl)biphenyl, N̂N̂CH=6-phenyl-2,2′-bipyridine, N̂CHN̂ = 1,3-di(2-pyridyl)benzene) was undertaken under the ab initio and the density functional theory (DFT) level. We carried out the present work with two goals: (1) to provide an in-depth theoretical understanding of the electronic structures and spectroscopic properties of **1**−**4** and (2) to explore the relationship between the shift of the spectra and the variation of pyridine ring. We hope that the exploration of

* Corresponding author. E-mail: zhanghx@mail.jlu.edu.cn.

10.1021/jp810965d CCC: $40.75
Published on Web 07/28/2009

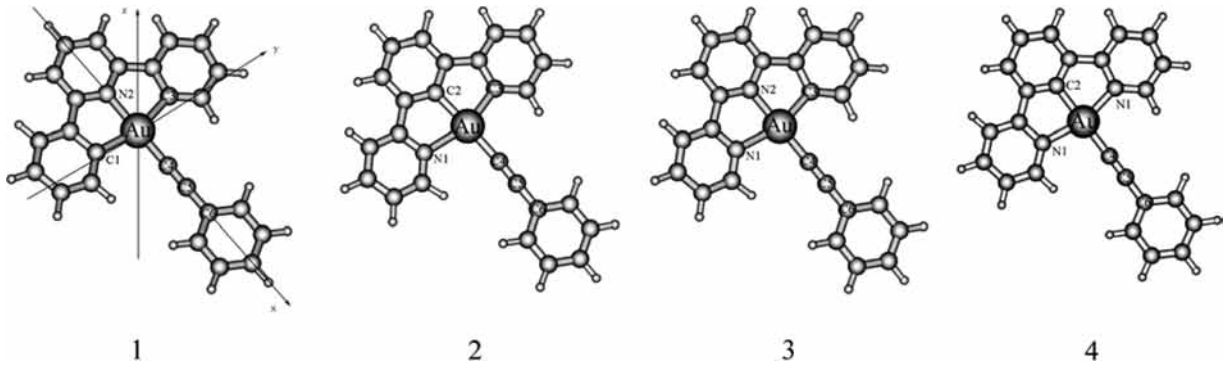

Figure 1. Optimized ground-state structures for **1**−**4** by the DFT(B3LYP) calculations.

TABLE 1: Partial Optimized Geometric Structural Parameters of 1−4 in the Ground and Excited States, Together with the Experimental Values of 1

	1			2		3		4	
parameters	$^1A_1$	$^3A_1$	exptl[a]	$^1A'$	$^3A'$	$^1A'$	$^3A'$	$^1A_1$	$^3A_1$
				Bond Lengths (Å)					
Au−N1				2.244	2.241	2.239	2.235	2.089	2.071
Au−N2	2.047	2.018	1.999			2.054	2.041		
Au−C1	2.099	2.075	2.073						
Au−C2				2.007	1.994			1.988	1.968
Au−C3	2.099	2.075	2.073	2.045	2.030	2.027	2.007		
Au−C4	1.968	1.988	1.979	2.052	2.079	1.962	1.975	2.047	2.062
C4−C5	1.219	1.197	1.185	1.224	1.230	1.219	1.218	1.224	1.201
C5−C6	1.428	1.441	1.439	1.427	1.379	1.427	1.386	1.428	1.441
				Bond Angles (deg)					
1-Au-2	80.5	80.8	81.0	77.5	77.6	76.4	76.5	79.5	79.3
1-Au-3	161.0	161.6	162.0	158.0	158.1	158.6	158.8	159.1	158.6
2−Au-C4	180.0	180.0	178.5	177.7	178.2	179.9	179.5	180.0	180.0
Au−C4−C5	180.0	180.0	176.6	177.5	177.7	177.4	176.7	180.0	180.0
C4−C5−C6	180.0	180.0	177.6	179.2	179.2	179.9	179.6	180.0	180.0

[a] From ref 9.

these characteristic properties for the gold(III) metal complexes will help us design good phosphorescent materials.

2. Computational Details and Theory

The density functional theory (DFT) at the Becke's three parameter functional and the Lee−Yang−Parr functional (B3LYP)[12] and single-excitation configuration interaction (CIS) methods[13] are employed to optimize the ground (S_0) and excited state (T_1) structures for **1**−**4**, respectively. The ground and excited state calculations are symmetry-restricted to C_{2v} for **1** and **4** and C_s for **2** and **3**, respectively. On the basis of the optimized ground and excited states, the spectroscopic properties related to the absorption and emission in solution are obtained by the time-dependent density functional theory (TD-DFT)[14] at the B3LYP functional associated with the polarized continuum model (PCM).[15]

In the work, quasi-relativistic pseudopotentials of Au atoms proposed by Hay and Wadt[16] with 19 valence electrons were employed, and the LANL2DZ basis sets associated with the pseudopotential were adopted. The 6-31G(d) basis sets were adopted for H, C, and N atoms. To precisely describe the molecular properties, one additional *f*-type polarization function was implemented for Au ($\alpha = 0.20$).[17] It has been shown that such a polarization function on a heavy atom is necessary to obtain reasonable geometry structures and accurate spectroscopic properties.[18] The basis sets are taken as Au (8s6p3d1f/3s3p2d1f), C (10s4p1d/3s2p1d), N (10s4p1d/3s2p1d), and H (4s/2s), respectively. Thus, 425 basis functions and 192 electrons for **1**−**4** are included in the calculations. All of the calculations were accomplished by using the Gaussian03 software package on an Origin/3900 server.[19]

3. Results and Discussion

3.1. Geometry Structures of 1−4 in the Ground States. The optimized S_0 structures of **1**−**4**, along with the coordination axis, are depicted in Figure 1, and the corresponding important parameters together with the X-ray crystal diffraction data of **1**[9] are listed in Table 1. As reported by Yam and co-workers, the aryl ring and cyclometalated plane in the [Au(ĈN̂C)C≡CPh] molecule in the crystalline form tend to be perpendicular to each other. However, in the gas phase calculation, by taking into account the possible maximum π conjugation between the two π electron-rich planes, the total molecule should be coplanar in the absence of lattice packing. Wong and co-workers also adopt coplanar structures in their calculation.[9c] Moreover, our calculated results show that the energy differences between the two forms for **1**−**4** are quite small and the lowest-energy emission wavelength of **1** calculated from the coplanar ground-state structure is more reasonable and consistent with the experimental value. Therefore, in the latter calculation, only the coplanar structures for **1**−**4** are taken into account.

As reported in Table 1, the optimized bond lengths and bond angles for **1** in the ground state are in general agreement with the corresponding experimental values.[9] The calculated bond distances of Au−N2 (2.047 Å), Au−C1 (2.099 Å), Au−C3 (2.099 Å), and C4−C5 (1.219 Å) are overestimated by about 0.03 Å in comparison with the measured values, whereas the bond distances of Au−C4 (1.968 Å) and C5−C6 (1.428 Å) are

TABLE 2: Partial Molecular Orbital Compositions in the Ground States for 1, 2 in CH_2Cl_2 Solution under TD-DFT (B3LYP) Calculations

		1			
MO	*E* (eV)	Au	ĈN̂C	C≡CPh	bond type
$47a_1$	−0.7973	$27.2d_{x^2-y^2}$ + 4.3P	55.9	12.4	d(Au) + π*(ĈN̂C) + π*(C≡C)
$7a_2$	−1.6784		99.6		π*(ĈN̂C)
$11b_1$	−2.1582	6.1P + $1.1d_{yz}$	89.8	3.00	π*(ĈN̂C)
		HOMO−LUMO Energy Gap			
$10b_1$	−5.7177	$7.2d_{yz}$	2.90	88.7	d(Au) + π(C≡C) + π(Ph)
$34b_2$	−6.0641	6.3P + $7.8d_{xy}$	54.4	31.1	d(Au) + π(ĈN̂C) + π(C≡C)
$6a_2$	−6.1836	$7.0d_{xz}$	92.9		d(Au) + π(ĈN̂C)
$5a_2$	−6.6500	$7.4d_{xz}$	92.5		d(Au) + π(ĈN̂C)
$4a_2$	−6.7036			100	π(Ph)
$9b_1$	−6.8214		98.3		π(ĈN̂C)
		2			
MO	*E* (eV)	Au	N̂ĈC	C≡CPh	bond type
19a″	−1.0169	7.3P + $0.7d_{yz}$	82.7	9.30	π*(N̂ĈC)
18a″	−1.4509	2.5P	96.3	1.00	π*(N̂ĈC)
17a″	−2.0145	4.1P + $1.1d_{xz}$	93.3	1.50	π*(N̂ĈC)
		HOMO−LUMO Energy Gap			
16a″	−5.5250	$6.8d_{yz}$ + 1.4P	6.00	85.9	d(Au) + π(C≡C) + π(Ph)
15a″	−5.8997	$3.6d_{yz}$	94.0	2.10	π(N̂ĈC)
80a′	−6.3066	$6.0d_z^2$ + $4.6d_{xy}$	12.6	75.8	d(Au) + π(C≡C) + π(N̂ĈC)
14a″	−6.5496	$3.4d_{yz}$	95.4	1.10	π(N̂ĈC)
13a″	−6.6396			100	π(Ph)
12a″	−6.7136	$6.8d_{xz}$ + $3.6d_{yz}$	86.7	2.80	d(Au) + π(N̂ĈC)

TABLE 3: Partial Molecular Orbital Compositions in the Ground State for 3, 4 in CH_2Cl_2 Solution under TD-DFT (B3LYP) Calculations

		3			
MO	*E* (eV)	Au	N̂N̂C	C≡CPh	bond type
81a′	−3.4352	$30.1d_{xy}$ + 3.0P	53.0	13.9	d(Au) + π*(N̂N̂C) + π*(C≡C)
18a″	−3.4681	1.9P	97.5	0.50	π*(N̂N̂C)
17a″	−4.1196	4.7P	93.9	1.40	π*(N̂N̂C)
		HOMO−LUMO Energy Gap			
16a″	−6.7917	$6.4d_{yz}$	2.10	91.5	d(Au) + π(C≡C) + π(Ph)
15a″	−7.4410			100	π(Ph)
80a′	−7.9286	$8.5d_{xy}$ + $3.2d_{x^2-y^2}$	10.9	77.5	d(Au) + π(C≡C)
14a″	−8.0032	$3.6d_{xz}$	96.4		π(N̂N̂C)
13a″	−8.3529	$7.6d_{xz}$	89.5	2.80	d(Au) + π(N̂N̂C)
12a″	−8.8125	$9.8d_{yz}$	9.30	80.8	d(Au) + π(C≡C) + π(Ph)
		4			
MO	*E* (eV)	Au	N̂ĈN	C≡CPh	bond type
$12b_1$	−2.5318		98.2		π*(N̂ĈN)
$8a_2$	−2.8218		98.9		π*(N̂ĈN)
$7a_2$	−3.6015		99.0		π*(N̂ĈN)
$11b_1$	−3.7658	8.9P	89.2	1.9	π*(N̂ĈN)
$47a_1$	−3.8420	$31.6d_{xy}$ + 10.1S	55.6	2.7	π*(N̂ĈN) + d(Au)
		HOMO−LUMO Energy Gap			
$10b_1$	−6.6048	$5.5d_{xz}$	2.40	92.1	π(C≡C) + π(Ph)
$6a_2$	−7.3499			100.0	π(Ph)
$34b_2$	−7.7262	$7.2d_{xy}$	10.9	81.9	π(C≡C) + d(Au)
$5a_2$	−8.1716		99.3		π(N̂ĈN)
$9b_1$	−8.2312	$8.4d_{xz}$	82.9	8.7	π(N̂ĈN) + d(Au)

underestimated by about 0.02 Å. As expected to the d^8 configuration, the Au(III) coordination planes take on quasi-square conformation, and the calculated bond angles are closed to the experimental values. The discrepancy of the geometry structural data between the calculated and the measured values is reasonable and acceptable, since the environments of the complexes are different in the two cases: in the latter complex, the molecule is in a tight crystal lattice, while in the former complex, the molecule is free.

By comparing the complexes, we can see that the bond length of Au−N2 in **1** is shortened by about 0.197 Å compared with Au−N1 of **2**, the pyridine of which is located at the side of aryl ring. When there are two pyridine rings, the lateral Au−N1 bond of **3** is shortened by about 0.005 Å compared with Au−N1 in **2**, whereas the intermediate Au−N2 of **3** is elongated by about 0.007 Å compared with Au−N2 of **1**. When the two pyridine rings are all located at the side of the aryl ring, the bond length between the metal and the cyclometalated ligand are shorter than any bond in the same position in **1**−**3**. Compared with the experimental values of **1**, the calculated bond lengths of C4−C5 in **1**−**4** are all overestimated by about 0.04 Å, and the bond lengths of C5−C6 are underestimated by about

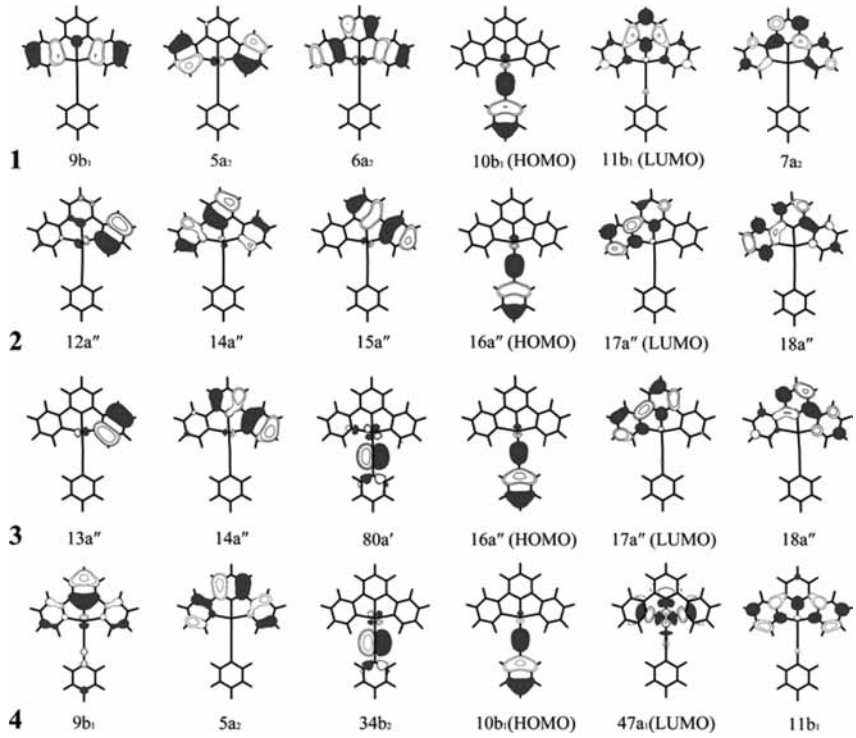

Figure 2. Electronic density diagrams of partial MOs in the ground state for **1**−**4**.

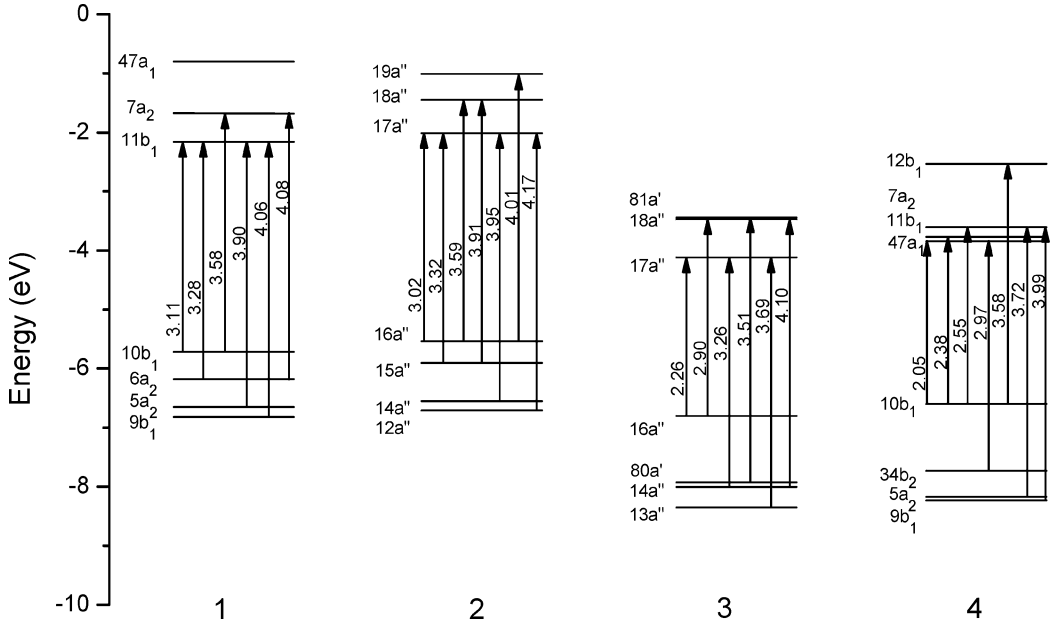

Figure 3. Diagrams of energy levels of partial molecular orbitals and the transitions responsible for the absorptions of **1**−**4** in CH_2Cl_2 solution under TD-DFT calculations.

0.01 Å. There are some contrary trends in the bond lengths: (1) The Au−C3 bond in **1** is 0.026 Å longer than the experimental values, whereas the bond lengths of **2** and **3** are 0.028 Å and 0.046 Å shorter, respectively. (2) The Au−C4 bond lengths of **2** and **4** are about 0.07 Å longer than the experimental values of **1**, but the bonds in **1** and **3** are 0.011 Å and 0.017 Å shorter, respectively. In a simple Dewar, Chatt, and Duncanson model,[20,21] the bond interaction between the metal and the ligand can be described as a donation from a σ molecular orbital of the ligand toward an empty d orbital of the metal and a concurrent back-donation from a filled (or partly filled) d orbital to a π^* antibonding orbital of the ligand. As we know, the electron-donating ability of a C atom in phenyl is stronger than a N atom in pyridyl for **1**−**4**, so the bond located trans to a N atom is shorter than that trans to a C atom. For the same reason, the complexes **2** and **3** adopt C_s point group rather than C_{2v} point group, which can be displayed in the variation of bond angles.

3.2. Absorption Spectra. The absorption spectra in CH_2Cl_2 solution for **1**−**4** are explored using the PCM model. It is well-known that the frontier molecular orbitals play a major role in the electronic transition, so we first reveal the frontier molecular orbitals for **1**−**4** (Tables 2 and 3). As seen in Tables 2 and 3, four conclusions can be drawn: (1) The virtual orbitals almost come from the cyclometalated ligands, except for the $47a_1$ (LUMO+2) of **1** (ca. 31.5% Au), 81a′ (LUMO+2) of **3** (ca. 30% Au), and $47a_1$ (LUMO) of **4** (ca. 42% Au). (2) The

TABLE 4: Absorptions of 1−4 in CH_2Cl_2 Solution According to TD-DFT Calculations, Together with the Experimental Values of 1

transition	excitation	coeff	E_{nm} (eV)	oscillator	assignment	exptl[a]/nm (ε_{max}/dm^3 mol^{-1}cm^{-1})
			1			
$X^1A_1 \rightarrow A^1A_1$	$10b_1 \rightarrow 11b_1$	0.70	398 (3.11)	0.1518	LLCT	402 (4870)
$X^1A_1 \rightarrow B^1B_2$	$6a_2 \rightarrow 11b_1$	0.68	378 (3.28)	0.0294	ILCT	381 (5870)
$X^1A_1 \rightarrow C^1B_2$	$10b_1 \rightarrow 7a_2$	0.70	346 (3.58)	0.0027	LLCT/MLCT	364 (5050)
$X^1A_1 \rightarrow D^1B_2$	$5a_2 \rightarrow 11b_1$	0.67	318 (3.90)	0.1097	ILCT	322 (19980)
$X^1A_1 \rightarrow E^1A_1$	$9b_1 \rightarrow 11b_1$	0.62	306 (4.06)	0.0471	ILCT	312 (19890)
$X^1A_1 \rightarrow F^1A_1$	$6a_2 \rightarrow 7a_2$	0.49	304 (4.08)	0.0676	ILCT/MLCT	
			2			
$X^1A' \rightarrow A^1A'$	$16a'' \rightarrow 17a''$	0.70	411 (3.02)	0.0727	LLCT	
$X^1A' \rightarrow B^1A'$	$15a'' \rightarrow 17a''$	0.68	373 (3.32)	0.0084	ILCT	
$X^1A' \rightarrow C^1A'$	$16a'' \rightarrow 18a''$	0.70	346 (3.59)	0.0259	LLCT/MLCT	
$X^1A' \rightarrow D^1A'$	$15a'' \rightarrow 18a''$	0.63	317 (3.91)	0.0850	ILCT	
$X^1A' \rightarrow E^1A'$	$14a'' \rightarrow 17a''$	0.53	314 (3.95)	0.0517	ILCT	
$X^1A' \rightarrow F^1A'$	$16a'' \rightarrow 19a''$	0.57	309 (4.01)	0.2564	LLCT	
$X^1A' \rightarrow G^1A'$	$12a'' \rightarrow 17a''$	0.64	298 (4.17)	0.0108	ILCT	
			3			
$X^1A' \rightarrow A^1A'$	$16a'' \rightarrow 17a''$	0.70	550 (2.26)	0.0838	LLCT	
$X^1A' \rightarrow B^1A'$	$16a'' \rightarrow 18a''$	0.70	428 (2.90)	0.0324	LLCT	
$X^1A' \rightarrow C^1A'$	$14a'' \rightarrow 17a''$	0.67	381 (3.26)	0.0473	ILCT	
$X^1A' \rightarrow D^1A'$	$80a' \rightarrow 81a'$	0.67	353 (3.51)	0.0282	LLCT/LMCT	
$X^1A' \rightarrow E^1A'$	$13a'' \rightarrow 17a''$	0.68	336 (3.69)	0.0646	ILCT	
$X^1A' \rightarrow F^1A'$	$14a'' \rightarrow 18a''$	0.56	302 (4.10)	0.1550	ILCT	
			4			
$X^1A_1 \rightarrow A^1A_1$	$10b_1 \rightarrow 11b_1$	0.69	522 (2.38)	0.0891	LLCT	
$X^1A_1 \rightarrow B^1B_2$	$10b_1 \rightarrow 7a_2$	0.70	485 (2.55)	0.0090	LLCT	
$X^1A_1 \rightarrow C^1B_2$	$34b_2 \rightarrow 47a_1$	0.70	418 (2.97)	0.0048	LLCT/LMCT	
$X^1A_1 \rightarrow D^1A_1$	$10b_1 \rightarrow 12b_1$	0.70	347 (3.58)	0.0354	LLCT	
$X^1A_1 \rightarrow E^1B_2$	$5a_2 \rightarrow 11b_1$	0.66	333 (3.72)	0.0431	ILCT	

[a] From ref 9.

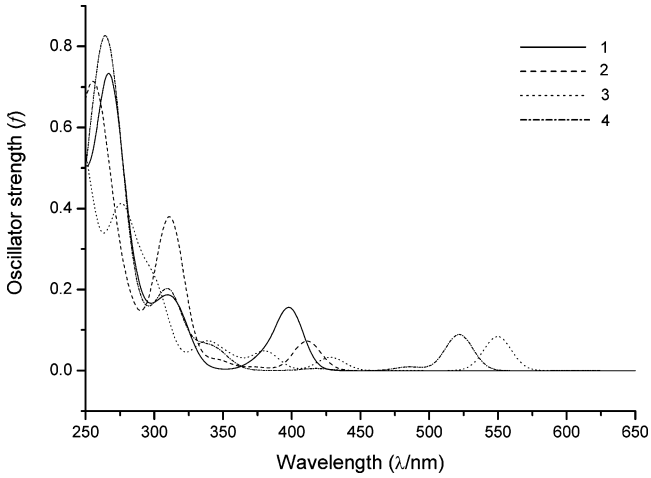

Figure 4. Simulated absorption spectra of **1**−**4** in CH_2Cl_2 solution.

TABLE 5: Natural Charge Analysis for 1−4 in the Ground States, Together with the HOMO-LUMO Energy Gaps

	1	2	3	4
Au	1.12231	1.06934	1.13323	1.24427
Pyridyl	0.05667	0.09687	0.62635	0.56850
Phenyl	−0.72470	−0.54980	−0.25643	−0.24049
C≡CPh	−0.45428	−0.61189	−0.50314	−0.57229
H≡L Gap (eV)	3.56	3.51	2.67	2.76

occupied orbitals are basically dominated by the ligands. The HOMO-2, HOMO-3, and HOMO-5 of **1** all come from the cyclometalated ligands. In addition, there are some orbitals localized on the cyclometalated plane for **2**−**4**, which are the HOMO-1, HOMO-3, and HOMO-5 of **2**, HOMO-3 and HOMO-4 of **3**, and HOMO-3 and HOMO-4 of **4**, respectively. (3) The HOMOs $10b_1$ (**1**), $16a''$ (**2**), $16a''$ (**3**), and $10b_1$ (**4**) have

TABLE 6: Phosphorescent Emissions of 1−4 in CH_2Cl_2 Solution According to TD-DFT (B3LYP) Calculations, Together with the Experimental Values of 1

	transition	configuration	coeff	E (nm) (eV)	assignment	exp[a] (nm)
1	$^3A_1 \rightarrow {}^1A_1$	$6a_2 \rightarrow 11b_1$	0.71	477 (2.60)	^{3}ILCT	476
		$9b_1 \rightarrow 7a_2$	−0.19		^{3}ILCT	
2	$^3A' \rightarrow {}^1A'$	$16a'' \rightarrow 20a''$	0.48	517 (2.40)	^{3}LLCT/^{3}ILCT	
		$16a'' \rightarrow 19a''$	−0.43		^{3}LLCT/^{3}ILCT	
		$16a'' \rightarrow 17a''$	−0.41		^{3}ILCT	
3	$^3A' \rightarrow {}^1A'$	$16a'' \rightarrow 17a''$	0.70	634 (1.96)	^{3}LLCT	
		$16a'' \rightarrow 20a''$	0.16		^{3}LLCT/^{3}ILCT	
4	$^3A_1 \rightarrow {}^1A_1$	$10b_1 \rightarrow 47a_1$	0.70	577 (2.15)	^{3}LLCT/^{3}LMCT	

[a] From ref 9.

a similar composition, which are composed of approximately 90% (C≡CPh) and 7% (Au). There is an absolute π(Ph) orbital for **1**−**4**, which is the HOMO-4 of **1**, **2** and HOMO-1 of **3**, **4**. (4) The composition of Au atomic orbitals is less than 10% in the high-energy occupied orbitals except for the HOMO-1 (14.1%) of **1**. In addition, the largest Au composition in high-energy occupied orbitals is 10.6% (HOMO-2) for **2**, 11.7% (HOMO-2) for **3**, and 8.4% (HOMO-4) for **4**. From this point, we can see that the composition of Au in frontier molecular orbital is very small, therefore the d-d excited state is unavailable and does not lead to nonradiative decay. This may be the reason that the alkynylgold(III) complexes could luminesce at both room temperature and 77 k.

To help us understand the orbitals described above, the electronic density diagrams of which are presented in Figure 2 and the orbital energy levels for **1**−**4** are illustrated in Figure 3. Table 4 gives the absorption data in terms of the transition states, excitation energies, excitations with maximum CI coefficients, oscillator strengths for **1**−**4** in CH_2Cl_2 solution, and the experimental values of **1**. For clarity, we list in Table 4

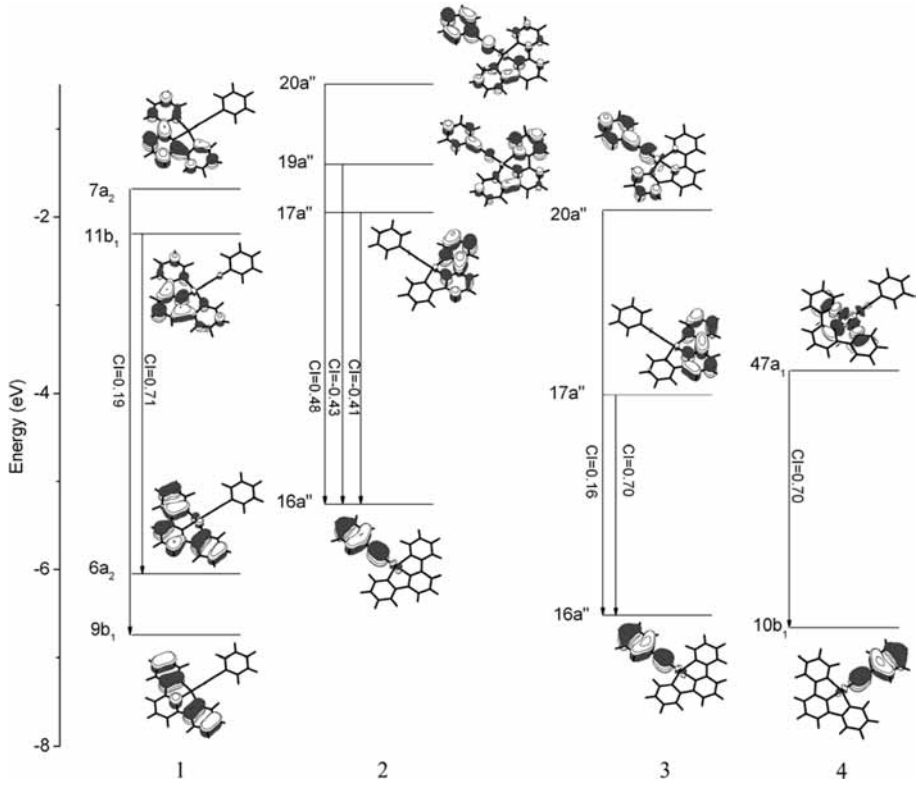

Figure 5. Single-electron transitions with |CI coefficients| > 0.1 according to TD-DFT calculations for the 477, 517, 634, and 577 nm of **1**−**4,** respectively, simulated in CH_2Cl_2 solution.

only the most leading excited states with the largest |CI coefficients|. Furthermore, we simulated the absorption spectra of **1**−**4** with a Gaussian-type curve in Figure 4. As revealed in Table 4, the lowest-lying dipole-allowed absorptions are at 398, 411, 550, and 522 nm for **1**−**4**, respectively, in which the leading excitation configuration of HOMO → LUMO is responsible for the transitions except the HOMO → LUMO+1 transition of **4**. As mentioned above, the HOMOs $10b_1$ (**1**), 16a″ (**2**), 16a″ (**3**), and $10b_1$ (**4**) are composed of approximately 90% (C≡CPh), whereas the LUMOs of **1**−**3** and LUMO+1 of **4** are mainly localized on the cyclometalated ligands. Therefore, the lowest-energy absorptions of **1**−**4** are attributed to LLCT. In Figure 4, we can clearly find that the lowest-energy absorption bands of **1**−**4** are red-shifted in the order **1** < **2** < **4** < **3**. The rest of the calculated absorptions of **1**−**4** can be seen in Table 4 and Figure 3.

To explore the nature of the shift order, we list the nature bond orbital (NBO)[22] analysis for **1**−**4** in Table 5 in terms of Au(III), pyridyl, phenyl, and phenylacetylide ligands, respectively. With respect to **1** and **2**, the Au(III) atom becomes less positively charged and the pyridyl becomes more positively charged. Moreover, the HOMO−LUMO energy gap of **1** is 3.56 and 0.05 eV higher than that of **2** (3.51 eV). This indicates that when the pyridyl is located at the side of aryl ring, the electron-accepting ability of pyridyl is bigger and the HOMO−LUMO energy gap of **2** (3.51 eV) is less than that of **1** (3.56 eV). The lowest-energy absorption band of **2** is red-shifted relative to **1**. With regard to **3** and **4**, there are two pyridyl. In complex **3**, the electronic charges residing on Au(III) and pyridyl are 1.13323 and 0.62635, and those in **4** are 1.24427 and 0.56850, respectively. In addition, the HOMO−LUMO energy gap of **3** (2.67 eV) is less than that of **4** (2.76 eV). This shows that the bipyridine-like unit in **3** is a good electron acceptor and thus ensures a low-energy LUMO. By comparing the complexes, we can get a conclusion that, with the variation in position and the number of pyridyl, the electron-accepting ability of pyridyl increases in the order **1** < **2** < **4** < **3** and the HOMO−LUMO energy gaps lowered correspondingly, which also corresponds to the order of the lowest-energy absorptions of **1**−**4** (**1** < **2** < **4** < **3**).

3.2.1. Solvent Effects. It is worth noting that differences in solvent polarity will dramatically influence the MO energies in solutions, hence, change the transition energy. Therefore, to compare the absorptions in media with different polarities, the absorptions for **1**−**4** in CH_3CN solution were also calculated, and the results are listed in Supporting Information, Table S1. Table S1 shows that, when the solvent is changed from CH_2Cl_2 to CH_3CN, the characters of absorptions are completely unchanged. But the lowest-energy absorptions in CH_3CN solution for **1**−**4** have slight change in energy, which are increased by 0.02, 0.02, 0.04, and 0.03 eV, respectively.

3.3. Excited-State Structures of 1−4. On the basis of the optimized ground-state structures, the lowest-energy excited-state structures of **1**−**4** are fully optimized out by the CIS method. The main geometry parameters of **1**−**4** in the excited state are presented in Table 1. As shown in Table 1, the bond angles of **1**−**4** in the excited state are almost identical to those in the ground-state, whereas the bond lengths have a minor change. The bond lengths between Au and cyclometalated ligand of **1**−**4** slightly shorten approximately 0.01−0.03 Å compared with those in the ground state, but the Au−C4 bond lengths of **1**−**4**, which connect the metal and the alkyne, are elongated approximately 0.01−0.03 Å. The variation of bond lengths indicates that the electrons are promoted from (−C≡CPh) ligand to cyclometalated ligand and the interaction between the Au atom and (−C≡CPh) ligand is weakened upon excitation. The C≡C bond of **1** and **3** are shortened by about 0.023 Å and 0.002 Å, respectively, while the triplet bond is elongated 0.006 Å and

0.002 Å in **2** and **4**, respectively. This indicates that the characters of the CT transitions occurring in **1**−**4** must be different.

3.4. Emission Spectra. In order to obtain the convincing emission energy, based on the excited-state structures optimized by the CIS method, the emission spectra of **1**−**4** in CH_2Cl_2 solution are calculated by the TD-DFT approach at the B3LYP level. The corresponding emissions of **1**−**4** are listed in Table 6, associated with the emission energies, transition assignments, and the experimental values of **1**.[9] To conveniently discuss the transition property of emission, we present the compositions and the electronic density diagrams of partial molecular orbitals related to the emissions in Supporting Information, Table S2 and Figure 5, respectively. In Table S2, we can see that the compositions of HOMOs are similar to each other in **1**−**4**, which have approximately 90% (C≡CPh), whereas the LUMOs are mainly localized on the cyclometalated ligands except **4**, which has 41.5% Au.

The calculated emissions in CH_2Cl_2 solution are 477, 517, 634, and 577 nm, respectively. As shown in Table 6, the emission at 477 nm of **1** is mainly from the transitions of MO $6a_2$ (HOMO-1) → MO $11b_1$ (LUMO) and MO $9b_1$ (HOMO-5) → MO $7a_2$ (LUMO+1) configurations with CI coefficients 0.71 and −0.19, respectively. As seen in Table S2, the HOMO-1 ($6a_2$) and LUMO ($11b_1$) are composed of 93.1% π(ĈN̂C) and 89.5% π*(ĈN̂C), respectively. Thus, the transition of $6a_2$ → $11b_1$ with CI coefficient 0.71 is assigned as ^{3}ILCT. Similar to that, the transition $9b_1$ → $7a_2$ is also attributed to ^{3}ILCT with the molecular orbital located at the (ĈN̂C) plane. With respect to **2**, as seen in Table 6, the emission at 517 nm is from three transitions with CI coefficients 0.48, −0.43, and −0.41, respectively. In Figure 5, the electron density diagrams of the frontier molecular orbitals of **2** intuitively illustrate that the 517 nm emission arises from the ^{3}ILCT combined by ^{3}LLCT. For **3**, the calculated lowest-energy emission occurs at 634 nm in CH_2Cl_2 solution with the nature of a $^3A' \rightarrow {}^1A'$ transition. In the transition, the triplet excited-state configurations of 16a″ (HOMO) → 17a″ (LUMO) and 16a″ (HOMO) → 20a″ (LUMO+4) with the coefficients 0.70 and 0.16 contribute to the transition. As seen in Table S2, the HOMO (16a″) is composed of 92.2% [π(C≡C) + π(Ph)], while the LUMO (17a″) is mainly localized on the N̂N̂C plane, and the LUMO+4 (20a″) is composed of about 32.2% π*(N̂N̂C), 52.2% π*(Ph), and 15.5% P(Au). So the emission at 634 nm for **3** is assigned to the combined transitions of ^{3}LLCT and ^{3}ILCT. For **4**, as mentioned above, the HOMO ($10b_1$) is composed of 93.1% [π(C≡C) + π(Ph)], whereas the LUMO ($47a_1$) has 41.5% Au and 55.9% π*(N̂ĈN). So the transition of $10b_1$ → $47a_1$ with CI coefficient 0.70 is assigned as ^{3}LLCT/^{3}LMCT. To intuitively understand the nature of the emissions, diagrams of the single-electron transitions related to the phosphorescence of **1**−**4** are shown in Figure 5.

4. Conclusions

Electronic structures and spectroscopic properties of **1**−**4** were investigated theoretically. We calculated their absorption and emission spectra in CH_2Cl_2 solution using the TD-DFT method with the PCM solvent model. By taking into account the effect of position and the number of pyridyl, the following conclusions can be drawn: The optimized geometric parameters of **1**−**4** in the ground state are in agreement with the experimental measured values. Upon excitation, the bond lengths between Au and cyclometalated ligands are shortened, whereas the bond lengths between Au and alkyne are elongated. This reflects that the electrons are promoted from the (−C≡CPh) ligand to the cyclometalated ligand. With the variation in position and the number of pyridyl, the electron-accepting ability of pyridyl increases in the order **1** < **2** < **4** < **3**, and the HOMO−LUMO energy gaps are lowered correspondingly. The lowest-energy absorption and emission bands of **1**−**4** are red-shifted in the order **1** < **2** < **4** < **3**. The calculations reveal that the lowest-lying absorptions for **1**−**4** are all derived from the LLCT. The lowest-energy emissions for **2** and **3** come from the ^{3}LLCT transition perturbed by some ^{3}ILCT transition, whereas the emissions for **1** and **4** are attributed to the ^{3}ILCT and ^{3}LLCT/^{3}LMCT, respectively. We hope these theoretical studies can provide some help in designing highly efficient phosphorescent materials.

Acknowledgment. This work is supported by the Natural Science Foundation of China (20333050, 20573042) and the Research Fund for the Doctoral Program of Higher Education (200801831004), China Postdoctoral Science Foundation (20080440149).

Supporting Information Available: The absorptions data in CH_3CN solution and the partial molecular orbital compositions in the lowest-energy excited state of **1**−**4** are listed in Tables S1 and S2, respectively. We also showed forty vertical transitions of **4** with excitation energies and oscillator strengths in CH_2Cl_2 absorption. This information is available free of charge via the Internet at http://pubs.acs.org.

References and Notes

(1) (a) Wand, Y.; Herron, N.; Grushin, V. V.; LeCloux, D. D.; Petrov, V. A. *Appl. Phys. Lett.* **2001**, *79*, 449. (b) Xin, H.; Li, F. Y.; Shi, M.; Bian, Z. Q.; Huang, H. C. *J. Am. Chem. Soc.* **2003**, *125*, 7166. (c) Tsuboyama, A.; Iwawaki, H.; Furugori, M.; Mukaide, T.; Kamatani, J.; Igawa, S.; Moriyama, T.; Miura, S.; Takiguchi, T.; Okada, S.; Hoshino, M.; Ueno, K. *J. Am. Chem. Soc.* **2003**, *125*, 12971. (d) Zhou, X.; Zhang, H. X. *J. Phys. Chem. A* **2005**, *109*, 8809. (e) Liu, T.; Xia, B. H.; Zhou, X.; Zhang, H. X.; Pan, Q. J.; Gao, J. S. *Organometallics* **2007**, *26*, 143.

(2) (a) Xiang, H. F.; Chan, S. C.; Wu, K. K. Y.; Che, C. M.; Lai, P. T. *Chem. Commun.* **2005**, *11*, 1408. (b) Pan, Q. J.; Fu, H. G.; Yu, H. T.; Zhang, H. X. *Inorg. Chim. Acta* **2006**, *359*, 3306.

(3) (a) Lamansky, S.; Djurovich, P.; Murphy, D.; Abdel-Razzaq, F.; Lee, H. E.; Adachi, C.; Burrows, P. E.; Forrest, S. R.; Thompson, M. E. *J. Am. Chem. Soc.* **2001**, *123*, 4304. (b) Wong, W. Y.; Zhou, G. J.; Yu, X. M.; Kwok, H. S.; Tang, B. Z. *Adv. Funct. Mater.* **2006**, *16*, 838. (c) Polson, M.; Ravaglia, M.; Fracasso, S.; Garavelli, M.; Scandola, F. *Inorg. Chem.* **2005**, *44*, 1282. (d) Williams, J. A. G.; Wilkinson, A. J.; Whittle, V. L. *Dalton Trans.* **2008**, *16*, 2081.

(4) (a) Tung, Y. L.; Wu, P. C.; Liu, C. S.; Chi, Y.; Yu, J. K.; Hu, Y. H.; Chou, P. T.; Peng, S. M.; Lee, G. H.; Tao, Y.; Carty, A. J.; Shu, C. F.; Wu, F. I. *Organometallics* **2004**, *23*, 3745. (b) Chou, P. T.; Chi, Y. *Eur. J. Inorg. Chem.* **2006**, 3319.

(5) (a) Tung, Y. L.; Lee, S. W.; Chi, Y.; Chen, L. S.; Shu, C. F.; Wu, F. I.; Carty, A. J.; Chou, P. T.; Peng, S. M.; Lee, G. H. *Adv. Mater.* **2005**, *17*, 1059. (b) Chen, C. Y.; Wu, S. J.; Li, J. Y.; Wu, C. G.; Chen, J. G.; Ho, K. C. *Adv. Mater.* **2007**, *19*, 3888.

(6) (a) Masahisa, O.; Mikio, H.; Daisuke, H. *Chem. Phys. Lett.* **2007**, *436*, 89. (b) Lee, Y. A.; McGarrah, J. E.; Lachicotte, R. E.; Eisenberg, R. *J. Am. Chem. Soc.* **2002**, *124*, 10662.

(7) (a) Vicente, J.; Juan, G. R.; Natalia, B.; Peter, G. J.; Delia, B. *Organometallics* **2008**, *27*, 646. (b) Ho, S. Y.; Cheng, E. C. C.; Tiekink, E. R. T.; Yam, V. W. W. *Inorg. Chem.* **2006**, *45*, 8165. (c) Che, C. M.; Chao, H. Y.; Miskowski, V. M.; Cheung, K. K. *J. Am. Chem. Soc.* **2001**, *123*, 4985. (d) Tzeng, B. C.; Yeh, H. T.; Huang, Y. C.; Chao, H. Y.; Lee, G. H.; Peng, S. M. *Inorg. Chem.* **2003**, *42*, 6008.

(8) (a) Yam, V. W. W.; Choi, S. W. K.; Lai, T. F.; Lee, W. K. *J. Chem. Soc., Dalton Trans.* **1993**, 1001. (b) Chan, C. W.; Wong, W. T.; Che, C. M. *Inorg. Chem.* **1994**, *33*, 1266. (c) Wong, K. H.; Cheung, K. K.; Chan, M. C. W.; Che, C. M. *Organometallics* **1998**, *17*, 3505.

(9) (a) Yam, V. W. W.; Wong, K. M. C.; Hung, L. L.; Zhu, N. *Angew. Chem., Int. Ed.* **2005**, *44*, 3107. (b) Wong, K. M. C.; Zhu, X. L.; Hung, L. L.; Zhu, N.; Yam, V. W. W.; Kwok, H. S. *Chem. Commun.* **2005**, 2906. (c) Wong, K. M. C.; Hung, L. L.; Lam, W. H.; Zhu, N.; Yam, V. W. W. *J. Am. Chem. Soc.* **2007**, *129*, 4350.

(10) (a) Yam, V. W. W.; Tang, R. P. L.; Wong, K. M. C.; Cheung, K. K. *Organometallics* **2001**, *20*, 4476. (b) Yam, V. W. W.; Wong, K. M. C.; Zhu, N. *J. Am. Chem. Soc.* **2002**, *124*, 6506. (c) Wong, K. M. C.; Tang, W. S.; Lu, X. X.; Zhu, N.; Yam, V. W. W. *Inorg. Chem.* **2005**, *44*, 1492.

(11) (a) Lu, W.; Mi, B. X.; Chan, M. C. W.; Hui, Z.; Che, C. M.; Zhu, N.; Lee, S. T. *J. Am. Chem. Soc.* **2004**, *126*, 4958. (b) Zhou, X.; Pan, Q. J.; Xia, B. H.; Li, M. X.; Zhang, H. X.; Tung, A. U. *J. Phys. Chem. A* **2007**, *111*, 5465.

(12) (a) Becke, A. D. *J. Chem. Phys.* **1993**, *98*, 5468. (b) Stevens, P. J.; Devlin, J. F.; Chabalowski, C. F.; Frisch, M. J. *J. Phys. Chem.* **1994**, *98*, 11623. (c) Becke, A. D. *Phys. Rev. A* **1988**, *38*, 3098. (d) Lee, C.; Wang, W.; Parr, R. G. *Phys. Rev. B* **1988**, *37*, 785.

(13) (a) Stanton, J. F.; Gauss, J.; Ishikawa, N.; Head-Gordon, M. *J. Chem. Phys.* **1995**, *103*, 4160. (b) Foreman, J. B.; Head-Gordon, M.; Pople, A. *J. Phys. Chem.* **1992**, *96*, 135. (c) Waiters, V. A.; Hadad, C. M.; Thiel, Y.; Colson, S. D.; Wibergy, K. B.; Johnson, P. M.; Foresmanl, J. B. *J. Am. Chem. Soc.* **1991**, *113*, 4782.

(14) (a) Casida, M. E.; Jamorski, C.; Casida, K. C.; Salahub, D. R. *J. Chem. Phys.* **1998**, *108*, 4439. (b) Stratmann, R. E.; Scuseria, G. E. *J. Chem. Phys.* **1998**, *109*, 8218. (c) Matsuzawa, N. N.; Ishitani, A. *J. Phys. Chem. A* **2001**, *105*, 4953.

(15) (a) Cossi, M.; Scalmani, G.; Regar, N.; Barone, V. *J. Chem. Phys.* **2002**, *117*, 43. (b) Barone, V.; Cossi, M. *J. Chem. Phys.* **1997**, *107*, 3210.

(16) (a) Wadt, W. R.; Hay, P. J. *J. Chem. Phys.* **1985**, *82*, 284. (b) Hay, P. J.; Wadt, W. R. *J. Chem. Phys.* **1985**, *82*, 299.

(17) Pyykkö, P.; Mendizabal, F. *Inorg. Chem.* **1998**, *37*, 3018.

(18) Pan, Q. J.; Zhang, H. X. *Inorg. Chem.* **2004**, *43*, 593.

(19) Frisch, M. J.; Trucks, G. W.; Schlegel, H. B.; Scuseria, G. E.; Robb, M. A.; Cheeseman, J. R.; Montgomery, J. A., Jr.; Vreven, T.; Kudin, K. N.; Burant, J. C.; Millam, J. M.; Iyengar, S. S.; Tomasi, J.; Barone, V.; Mennucci, B.; Cossi, M.; Scalmani, G.; Rega, N.; Petersson, G. A.; Nakatsuji, H.; Hada, M.; Ehara, M.; Toyota, K.; Fukuda, R.; Hasegawa, J.; Ishida, M.; Nakajima, T.; Honda, Y.; Kitao, O.; Nakai, H.; Klene, M.; Li, X.; Knox, J. E.; Hratchian, H. P.; Cross, J. B.; Bakken, V.; Adamo, C.; Jaramillo, J.; Gomperts, R.; Stratmann, R. E.; Yazyev, O.; Austin, A. J.; Cammi, R.; Pomelli, C.; Ochterski, J. W.; Ayala, P. Y.; Morokuma, K.; Voth, G. A.; Salvador, P.; Dannenberg, J. J.; Zakrzewski, V. G.; Dapprich, S.; Daniels, A. D.; Strain, M. C.; Farkas, O.; Malick, D. K.; Rabuck, A. D.; Raghavachari, K.; Foresman, J. B.; Ortiz, J. V.; Cui, Q.; Baboul, A. G.; Clifford, S.; Cioslowski, J.; Stefanov, B. B.; Liu, G.; Liashenko, A.; Piskorz, P.; Komaromi, I.; Martin, R. L.; Fox, D. J.; Keith, T.; Al-Laham, M. A.; Peng, C. Y.; Nanayakkara, A.; Challacombe, M.; Gill, P. M. W.; Johnson, B.; Chen, W.; Wong, M. W.; Gonzalez, C.; Pople, J. A. *Gaussian 03*, revision C.02; Gaussian, Inc.: Wallingford, CT, 2004.

(20) Dewar, M. J. S. *Bull. Soc. Chim. Fr.* **1951**, *18*, C71.

(21) Chatt, J.; Duncanson, L. A. *J. Chem. Soc.* **1953**, 2939.

(22) (a) Reed, A. E.; Weinstock, R. B.; Weinhold, F. *J. Chem. Phys.* **1985**, *83*, 735. (b) Foster, J. P.; Weinhold, F. *J. Am. Chem. Soc.* **1980**, *102*, 7211.

JP810965D